Rino *et al. Earth, Planets and Space* (2023) 75:64
https://doi.org/10.1186/s40623-023-01823-6

Earth, Planets and Space

FULL PAPER

Open Access

A three-dimensional stochastic structure model derived from high-resolution isolated equatorial plasma bubble simulations

Charles Rino[1*], Tatsuhiro Yokoyama[2] and Charles Carrano[1]

Abstract

Ionospheric structure is characterized by the space–time variation of electron density. However, our understanding of the physical processes that initiate and sustain intermediate-scale structure development does not relate directly to statistical measures that characterize the structure. Consequently, high-resolution physics-based equatorial plasma bubble simulations are essential for identifying systematic relations between statistical structure measures and the underlying physics that initiates and sustains the structure evolution. An earlier paper summarized the analysis of simulated equatorial plasma bubble (EPB) structure initiated with a quasi-periodic bottom-side perturbation that generated five plasma bubbles. The results are representative of real environments. However, the association of the structure development with individual EPBs was difficult to ascertain. This paper summarizes the analysis of new results from single isolated EPB realizations with varying parameters that affect the structure development. The evolution of the single isolated EPB realizations reveal what we have identified as a canonical structure evolution pattern manifest in the space–time development of four quantitative spectral parameters. The onset of structure occurs when the plasma bubble penetrates the F-region peak. The parameter evolution from the initiation point have a fish-like appearance. The three-dimensional structure model can be used to interpret in situ and remote diagnostic measurements as well as predicting the deleterious effects of propagation disturbances on satellite communication, navigation, and surveillance systems.

Keywords Equatorial Spread F, Power-law ionospheric structure, Convective plasma instability, Structure characterization

*Correspondence:
Charles Rino
charles.rino@bc.edu
Full list of author information is available at the end of the article

Graphical Abstract

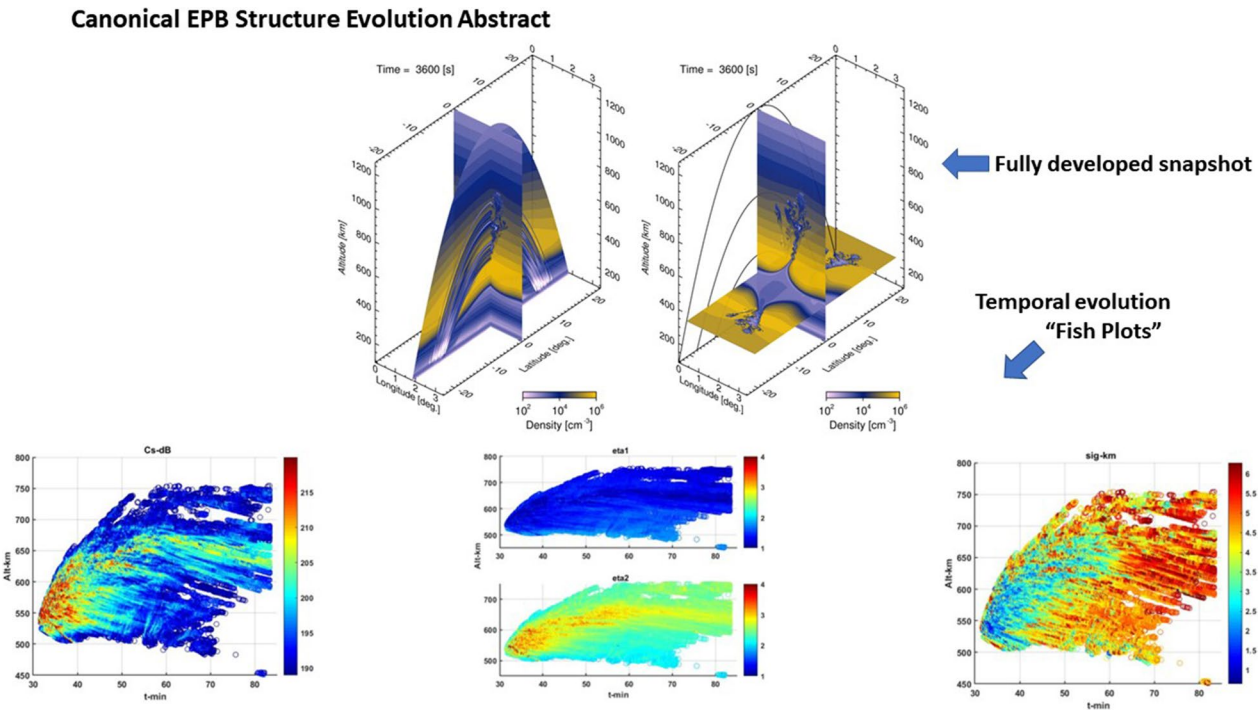

Introduction

Although the ionosphere is an extremely complex system, electron density, $N_e(\mathbf{r}, t)$, is a sufficient observable for structure characterization separate from the state of the ionosphere and underlying physics. We consider a region of interest (ROI) centered on a GPS coordinate, $\mathbf{r}_0$, with temporal evolution initiated at universal time, t_0. We let

$$N_e(\mathbf{r}, t) = \bar{N}_e(\mathbf{r}_0, t_0) + DN_e(\Delta\mathbf{r}, \Delta t), \tag{1}$$

where the *background* electron density, $\overline{N}_e(\mathbf{r}_0, t_0)$, is derived from a global ionospheric model and $DN_e(\Delta\mathbf{r}, \Delta t)$ represents a class of structure that supports statistical measures. Formally,

$$DN_e(\Delta\mathbf{r}, \Delta t) \simeq \Delta N_e(\mathbf{v}_{\text{eff}}\Delta t) + \delta N_e(\Delta\mathbf{r}, \Delta t). \tag{2}$$

The term $\Delta N_e(\mathbf{v}_{\text{eff}}\Delta t)$ represents intermediate-scale structure that evolves slowly enough to support spatially invariant configurations over measurement intervals. The term δN_e represents diffusive process that removes structure at small scales.

In situ probes measure electron density directly. Electromagnetic waves that propagate through the ionosphere can be processes to measure path-integrated electron density. Either way, an effective scan velocity, $\mathbf{v}_{\text{eff}}$, translates intercepted spatial structure to a time varying form that can be manipulated to generate representative diagnostic time series.

The structure model represented by (2) was developed to characterize stochastic structure. The remainder of this paper will address structure associated with the phenomenon know as Equatorial Spread F, which is an historical reference to anomalous ionogram signatures. Electron density depletions, commonly called equatorial plasma bubbles (EPBs), are the principal manifestations of spread F. High-resolution physics-based plasma simulations, as described in Yokoyama (2017), provide an ideal test-bed for quantitative stochastic structure characterization.

Homogeneous stochastic structure can be characterized by a spectral density function (SDF), which is formally the average intensity of a spatial Fourier decomposition of the structure. In an earlier study (Rino et al. 1918) published in situ and remote structure measurements led us to postulate a one-dimensional SDF of the form

$$\Phi_{\Delta N_e}(q_s) = C_s \begin{cases} q_s^{-\eta_1} & \text{for } q_s \le q_0 \\ q_0^{\eta_2-\eta_1} q_s^{-\eta_2} & \text{for } q_s > q_0 \end{cases}. \tag{3}$$

The variable q_s is spatial frequency measured in radians per meter. Four parameters; turbulent strength, C_s^1, the spectral indices, η_1, and η_2, and the break frequency, q_0 define the SDF. An iterative parameter estimation (IPE) procedure, which is described in Rino et al. (1918), was used to generate maximum likelihood estimates of the structure parameters.

The original study initiated an EPB structure realization with a bottom-side perturbation representative of a traveling ionospheric disturbance, which spawned five initially separated bubbles. The purpose of this paper is to present new results from single isolated EPB realizations. The new results characterize a canonical EPB structure evolution.

A three-dimensional structure model was developed to accommodate arbitrary orientations of the ROI relative to the magnetic field direction. Applications of the model for propagation diagnostics and performance analysis of satellite beacon, navigation, communication, and surveillance applications will be discussed in the discussion section. The next section summarizes the single-bubble results.

Results

Simulations were performed in an asymmetrically sampled dipole magnetic-field-aligned coordinate system. A bottom-side F-layer perturbation initiates 60-min EPB realizations. Uniformly spaced electron density samples were extracted from two-dimensional oblique slice planes. Each slice plane spans an altitude range from 300 to 800 km with a cross-field extent of 373.4 km. Altitude was sampled at 300.19-m intervals. The cross-field sample interval was 222.4 m. Periodograms were computed for each cross-field scan after trend removal. Trend removal is a necessary initial step that determines the largest resolved spatial scale within the ROI. In the original study 10 periodogram estimates were averaged prior to IPE parameter estimation. Slice planes were processed at 100-s intervals.

Rapid structure development was observed after rising EPBs penetrated the F-layer peak density. Once initiated, the structure development expands and progresses upward. An altitude sub-range that captures the developed structure is readily identified. Two-component SDFs with $\eta_1 \sim 1.5$ and $\eta_2 \sim 2.5$ were measured within the developed structure region. A single power-law with $\eta \sim 2$ was measured below the developed structure region. In the original study the structure break scale ($\sigma_0 = 2\pi/q_0$) varied from less than 1 km to more than 6 km with no clear pattern. The break-scale variability was attributed to commingling of the expanding EPB plumes. The same patterns were observed in slice-planes offset from the equatorial plane.

The single-bubble EPB simulations were processed with 10-s time resolution. PSD averaging is a compromise between uncertainty and altitude resolution. Based on the original results, the new results were processed with non overlapping averages of two PSD estimates to increase the altitude resolution. An applied electric field induces a 120 mps westward drift. Each frame was shifted to center the EPB in the frame. The left frame in Fig. 1 shows the new equatorial-plane EPB structure at 10-min intervals starting at 30 min, which captures the structure onset. The right frame shows zoomed views at 40-s intervals, which show the rapid structure onset. The developed left summary frames show enhanced

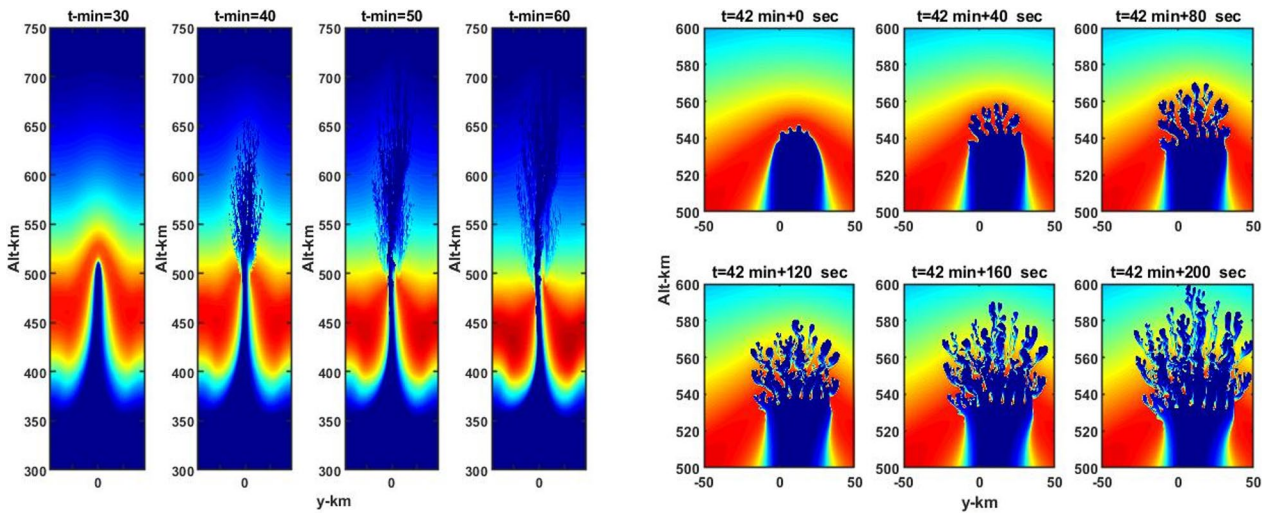

Fig. 1 The left frame summarizes the single-bubble development at 10-min intervals starting at the bubble penetration of the F-region peak. The color display scale is linear 0 to $10^{11}/m^3$. The right frame shows a zoomed 10-s sequence of the structure onset development

structure on the westward EPB wall at altitudes below the developed structure. This structure is attributed to secondary instability generated by the $E \times B$ drift of the wall gradient.

At structure onset quasi-periodic kilometer-scale voids penetrate the bubble cap followed by fractal-like finer scale structure development. The process is often described as successive bifurcation, which implies a doubling of the number of branches with half the parent structure dimension. The concentration of structure in the center of the slice-plane scans is ideally suited for spectral analysis. Each scan contains 1680 samples, from which the linear component connecting the end points has been removed. Discrete Fourier transforms (DFTs) are computed with zero padding to 1728 samples for efficient DFT computation. IPE parameter estimation was applied to averaged PSDs to generate the four structure parameter estimates.

The turbulent-strength parameter is used to identify structured slice-plane regions. The IPE parameters are well defined in the altitude range where *CsdB* is greater than 190 dB. Figure 2 shows the *CsdB* progression. Variance is determined by the integral of the SDF, which can be strongly influenced by the low spatial frequency contributions. However, as can be seen from the spectral-index parameters summarized in the upper frame of Fig. 3, the low-spatial frequency index is nearly invariant, whereby *CsdB* is a quantitative measure of the structure variance.

Figure 4 shows the progression of the break-scale estimates. Comparing, Figs. 2, 3, and 4 to the four frames in Rino et al. (1918). Figure 8 shows the improved definition of the structure evolution parameters, particularly the break scale. The single-bubble realization

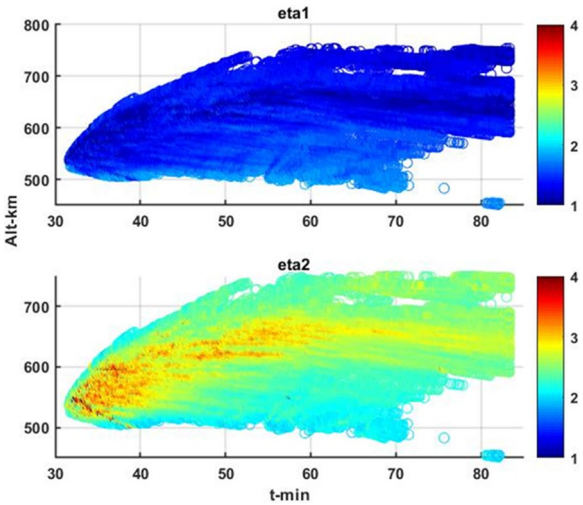

Fig. 3 Altitude-dependent EPB index-parameter (η1upper frame, η2 lower frame) evolution

shows that the break-scale varies inversely with turbulent strength in the high *CsdB* region. Below the lower boundary edge of the enhanced turbulent strength, the SDF transitions to a single power law.

Figure 5 shows probability distribution functions (PDFs) of the IPE parameters. The SDFs with $CsdB < 190$ dB are distorted by sidelobes of undeveloped EPB structure, as discussed in Rino et al. (1918). The σ_0 PDF shows two distinct peaks corresponding to the smaller and larger break scale populations. A definitive relation between the break scale and the scale associated with the structure onset remains to be demonstrated. Figure 6 shows the progression of the break scale in a 20 km altitude range centered at 550 km. The blue line is a least-squares second-order polynomial fit to the data. The break scale

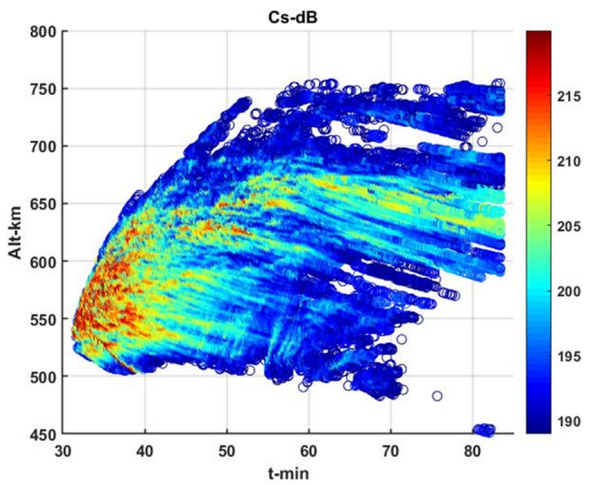

Fig. 2 EPB altitude-dependent turbulent-strength parameter evolution

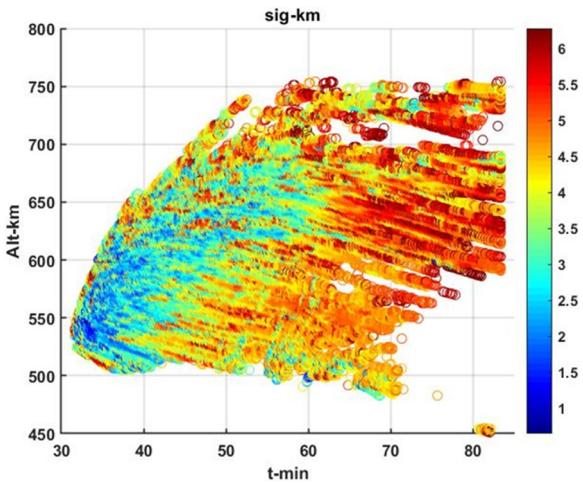

Fig. 4 Altitude-dependent EPB break-scale evolution

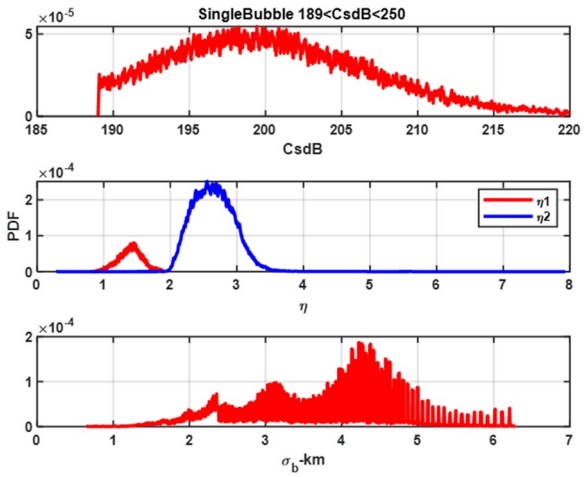

Fig. 5 Probability distributions of IPE parameters. (*CsdB* upper frame, $\eta 1, \eta 2$, middle frame, σ_b lower frame)

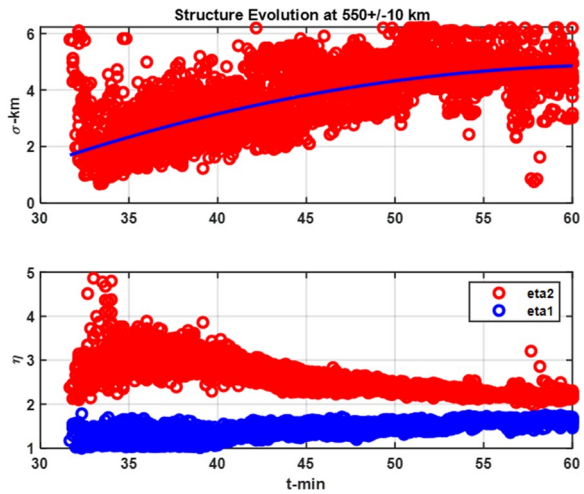

Fig. 6 Progression of height-dependent break scale (upper frame) and spectral index at 550 km

at initiation achieves is smallest value. As the structure spreads and decays the break scale increases.

Additional single-bubble simulations were generated with the ion content doubled and with the electric field reversed after initiation. Increased ion density slows the development but does not change the the canonical pattern. This can be seen qualitatively by comparing Fig. 7 to 1. The parameter summary plots shows the same canonical fish patterns, but delayed in time. Reversing the direction of the dynamo field suppressed the development, but did not change the overall fish patterns.

Figures 4 and 5 illustrate a canonical EPB structure development. Structure onset is initiated when the bubble cap penetrates the F-region peak. Enhanced turbulent strength spreads to higher altitudes defining the *fish* structure. The two-component inverse-power-law SDF starts with a shallow index, which transitions to a steeper index at a break scale that progressively decreases. Below the enhanced turbulence region a single power-law SDF characterizes the structure. The varying two-component power-law is confined to the structured region. A direct connection of defining SDF parameters to physical parameters that determine instability and initial growth rates has yet to be established.

Discussion

Although our analysis used structure snapshots, the progression of the structure development is slow enough to support the frozen structure hypothesis. An effective scan velocity allows conversion of the spatial structure to observable time series. A spatial structure model can be constructed by exploiting the fact that intermediate-scale structure is field aligned. Consequently, spatial stochastic structure is defined by the cross-field structure that intercepts the equatorial plane. For typical ROI dimensions the variation of the intercepting field-line direction can be neglected. The invariance of the simulation field-aligned structure was confirmed by comparing structure summaries in offset oblique slice planes in the original analysis.

Air glow, artificial barium releases, and the aurora support a structure model comprising striations, which are formally fixed radial ionization distributions that follow individual magnetic field lines. Each striation has a characteristic scale size and peak intensity. The defining cross-field structure of a randomly distributed configurations of striations is a two-dimensional isotropic SDF, $\Phi_{N_e}(q_y, q_z)$. It is readily shown that the measured SDF from a horizontal scan is defined by the integration

$$\Phi_{N_e}(q_y) = \int \Phi_{N_e}(q_y, q_z) \frac{dq_z}{2\pi}. \tag{4}$$

A commonly used method of constructing three-dimensional structure models starts with the isotropic spatial coherence function introduced by Shkarofsky (1968). Incorporating the quadratic form introduced by Singleton (1970), contours of constant correlation are transform to ellipsoidal surfaces. Striations are highly elongated ellipsoids. However, the model only accommodates a single power law. Moreover, the Shkarofosky model is acutely sensitive to large-scale and small-scale cutoff parameters that suppress power-law-index-dependent singular behavior at small scales and the decay at large scales, respectively.

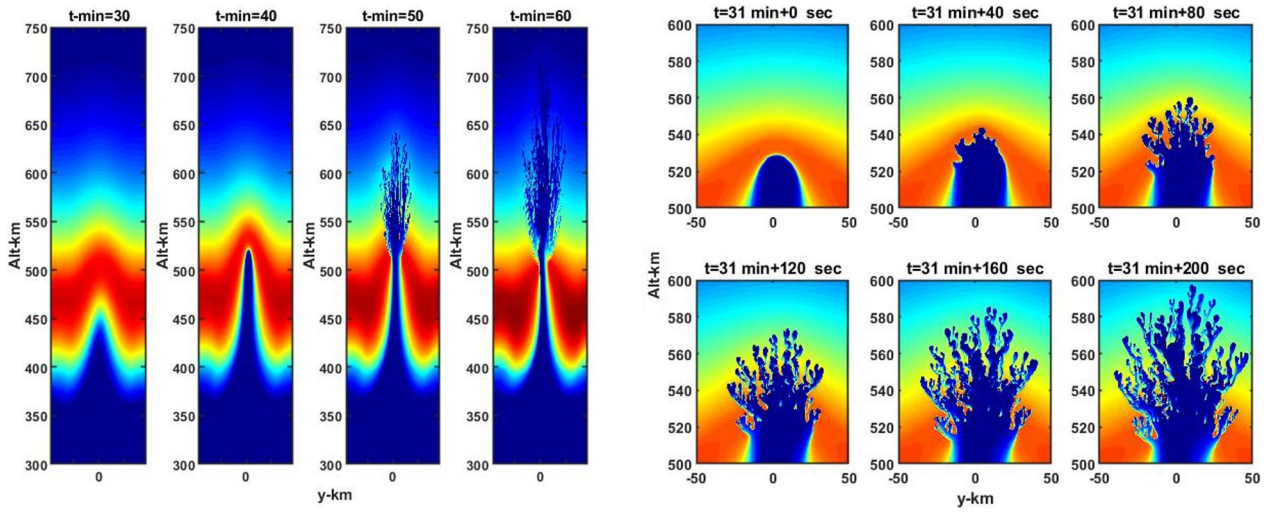

Fig. 7 Structure development summary for single-bubble realization with doubled ion density for comparison to Fig. 1

As an alternative, we introduced a configuration-space model comprising randomly distributed striations originating in a central slice plane (Rino et al. 2018). If the striations intercept the surface at an oblique angle, a rotation transforms the isotropic structure. For ellipsoidal striations, three-dimensional and two-dimensional spatial wave numbers are related as follows:

$$q_s^2 = \left(C\begin{matrix}\kappa_x\\ \kappa\end{matrix}\right)\left(C\begin{matrix}\kappa_x\\ \kappa\end{matrix}\right)^T. \tag{5}$$

The quadratic form defined by q_s is the spectral-domain form of Singleton's transformation. Although striations vary continuously, using a constant magnetic field direction approximates parallel structure within the ROI.

To accommodate a two-component inverse power law, we found that the size and intensity of the striations could be constructed to generate a two-component power law SDF (Rino et al. 2018). It is well known that power-law structure functions are associated with inverse power-law SDFs. The same relation connects the striation size and intensity to the power-law SDF wavelength and intensity. A realization of a canonical ESF structure is shown in Fig. 8. The blue curve is an average of one-dimensional PDFs. The two overlaid curves are the analytic (magenta) and the target (red) SDFs. The paper describes procedures for generating configurations with target SDFs and subsequent algorithmic computation of one-dimensional in situ and path-integrated SDFs. The defining relation is Equation (18) in Rino et al. (2018). The defining two-dimensional SDF, the three-dimensional SDF, and diagnostic one-dimensional SDFs all support two-component inverse power-law forms. The model reconciles the defining and measured inverse power-law parameters. For example, if p_n is the defining two-dimensional index, $\eta_n = p_n - 1$.

For path-integrated diagnostics structure, correlation along the integration path influences the result. The defining relation is

$$\Phi_{TEC}(\kappa_y) =; L\iint \frac{\sin(\kappa_x L/2)}{(\kappa_x L/2)^2}\Phi_{\Delta Ne}(\kappa_x,\kappa_y,\kappa_z)\frac{d\kappa_x}{2\pi}\frac{d\kappa_z}{2\pi}, \tag{6}$$

$$\simeq L\int \Phi_{\Delta Ne}(\kappa_y,\kappa_z)\frac{d\kappa_z}{2\pi}, \tag{7}$$

where L is the path length. The approximation assumes negligible decorrelation over the integration path. This assumption is used in scintillation models to relate the

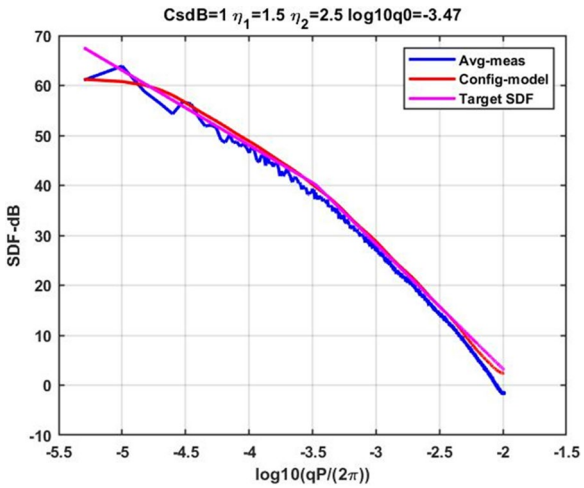

Fig. 8 One-dimensional SDF derived from configuration-space realization (blue), with target SDF (red) and configuration theoretical SDF (magenta) overlaid

weak-scatter intensity power-law index to an in situ index (Carrano and Rino 2016), which is the same as the two-dimensional to one-dimensional relation for direct electron density sampling.

To summarize, the IPE analysis procedure for estimating parameters that characterize a two-component power law can be applied to any in situ or TEC measurements. Early spectral analyses of C/NOFS satellite data (Rino et al. 2016) led to the application of IPE for the simulation studies. Although intermediate-scale structure associated with EPBs is responsible for for scintillation, the GNSS L-Band operating frequencies were chosen to eliminate the deleterious effects of scintillation. The diffraction contribution to signal GNSS signal phase is most often negligibly small. Moreover, when significant scintillation is present, the large-scale stochastic scintillation can be extracted and used to predict scintillation at other frequencies (Carrano et al. 2014).

Where definitive two-component signatures are observed, they can be interpreted against the canonical structure evolution. Where multiple structures are involved, canonical segments might still be identifiable. Nonuniform configuration structure realizations can be used to evaluate more complicated structures. Possibly nonuniform configurations could be incorporated in a model fitting procedure. For highly elongated structure striations are formally truncated at the ROI boundaries. Model results can be extracted for field-aligned propagation. However, the interpretation of such results is problematic unless curvature is taken into account.

The very large data base of GNSS TEC data is ideally suited for IPE parameter estimation. This was demonstrated with auroral zone GPS data, which had very weak scintillation but significant stochastic TEC variation (Rino et al. 2019). The term stochastic TEC refers to TEC structure unaffected by diffraction. A documented library of Matlab utilities for constructing and manipulating two-component inverse power-law models is available on request to the corresponding author.

Conclusions

Our results showed that fitting a two-component power-law SDF to physics-based realizations of evolving EPB structure reveal a canonical pattern. A structure model was introduced that can be applied to estimate defining cross-field structure parameters. Detailed descriptions and references can be found in Yokoyama (2017) and Rino et al. (1918). The next step is to apply the analysis to real data. Using models to remove geometric and propagation effects has a long history. Weak-scatter scintillation theory was used to derive probability of occurrence models of ionospheric structure (Vasylyev et al. 2022). More refined procedures have evolved which relate more directly to underlying physical processes Carrano et al. (2019), Carrano et al. (2018) Costa et al. (2011) and Bhattacharyya et al. (2016).

As noted in the discussion, we envision the IPE procedures as a complement to TEC structure analysis, which goes beyond EPB-initiated structure driven by processes that have their own canonical structure patterns. An example of IPE applied to auroral zone structure was presented in the discussion. Turbulence theory will most likely be needed to make direct connections to structure characteristics.

Abbreviations

EPB	Equatorial plasma bubble
SDF	Spectral density function
PSD	Power spectral density

Acknowledgements

The computation was performed on the FX100 supercomputer system at the Information Technology Center, Nagoya University and Hitachi SR16000/M1 system at NICT, Japan.

Author contributions

All of the simulations analyzed in this paper were performed by TY and generously reformatted and made available to CR who performed the analysis. The new results were initiated following analysis of the original simulations conceived by CR and TY at the December 2016 AGU meeting following a presentation by TY. CC has worked extensively to improve scintillation diagnostics, particularly definitive SDF parameter estimation, which was central to this study. All authors read and approved the final manuscript.

Funding

This work was supported by JSPS KAKENHI Grant Number JP16K17814. This work was also supported by the computational joint research program of the Institute for Space-Earth Environmental Research (ISEE), Nagoya University, Japan. Support for CR and CC was provided by internal research funding.

Declarations

Competing interests

The authors declare that they have no competing interest.

Author details

[1]Institute for Scientific Research, Boston College, 140 Commonwealth Ave., Chestnut Hill, MA 02467, USA. [2]National Institute of Information and Communications Technology, 4-2-1 Nukui-Kitamachi, Koganei, Tokyo 184-8795, Japan.

Received: 14 December 2022 Accepted: 15 April 2023
Published online: 28 April 2023

References

Bhattacharyya A, Kakad B, Gurram P, Sripathi S, Sunda S (2016) Development of intermediate scale structure at different altitudes within an equatorial plasma bubble: implications for L-band scintillations. J Geophys Res 122:1015

Carrano CS, Groves KM, Delay SH, Doherty PH (2014) An inverse diffraction technique for scaling measurements of ionospheric scintillations on the gps l1, l2, and l5 carriers to other frequencies. Proceedings of the 2014

Institute of Navigation ION ITM meeting, San Diego, California, January 27029, 2014
Carrano CS, Rino CL (2016) A theory of scintillation for two-component power law irregularity spectra: overview and numerical results. Radio Sci 51:789–813. https://doi.org/10.1002/2015RS005903
Carrano CS, Rino CL, Groves KM, Doherty PH (2018) A technique for inferring zonal irregularity drift from single-station GNSS measurements of intensity (s4) and phase (ϕ) scintillations. Radio Sci. https://doi.org/10.1002/2015RS005864
Carrano CS, Rino CL, Groves KM (2019) On the relationship between the rate of change of total electron content index (roti), irregularity strength (ckl), and the scintillation index (s4). J Geophys Res Space Phys 124:2099–2112. https://doi.org/10.1029/2018JA02635
Costa E, de Paula ER, de Rezende LFC, Groves KM, Roddy PA (2011) Equatorial scintillation predictions from c/nofs planar Langmuir probe electron density fluctuation data. URSI Gen Assembly Sci Sympos 2011:1–4. https://doi.org/10.1109/URSIGASS.2011.6050901
Rino C, Yokoyama T, Carrano C (1918) Dynamic spectral characteristics of equatorial plasma bubbles. Progr Earth Planet Sci. https://doi.org/10.1186/s40645-018-08243-0
Rino CL, Groves KM, Carrano CS, Roddy PA (2016) A characterization of intermediate-scale spread f structure from four years of high-resolution C/NOFS satellite data. Radio Science 51:19. https://doi.org/10.1002/2015RS005841
Rino C, Carrano C, Groves K, Yokoyama T (2018) A configuration space model for intermediate scale ionospheric structure. Radio Sci 53:1472. https://doi.org/10.1029/2018RS00667
Rino C, Morton Y, Breitsch B, Carrano C (2019) Stochastic tec structure characterzation. J Geophys Res Space Phys 124. https://doi.org/10.1029/2019JA026958
Shkarofsky IP (1968) Generalized turbulence space-correlation and wave-number spectrum-function pairs. Can J Phys 46:2133–2153
Singleton DG (1970) Saturation and focusing effects in radio-star and satellite scintillations. J Atmos Terr Phys 32:187–208
Vasylyev D, Béniguel Y, Volker W, Kriegel1 M, Berdermann J (2022) Modeling ionospheric scintillation. J Space Weather Space Clim 12 (22). https://doi.org/10.1051/swsc/2022016
Yokoyama T (2017) A review on the numerical simulation of equatorial plasma bubbles toward scintillation evaluation and forecasting. Prog Earth Planet Sci 4:37. https://doi.org/10.1186/s40645-017-0153-6

Publisher's Note